



Pergamon

Available online at [www.sciencedirect.com](http://www.sciencedirect.com)

SCIENCE @ DIRECT®

OCEAN  
ENGINEERING

Ocean Engineering 30 (2003) 1647–1667

[www.elsevier.com/locate/oceaneng](http://www.elsevier.com/locate/oceaneng)

## Burial and scour around short cylinder under progressive shoaling waves

S.I. Voropayev \*<sup>1</sup>, F.Y. Testik, H.J.S. Fernando, D.L. Boyer

*Environmental Fluid Dynamics Program, Department of Mechanical and Aerospace Engineering,  
Arizona State University, Tempe, AZ 85287-6106, USA*

Received 15 July 2002; accepted 18 October 2002

---

### Abstract

The results of a laboratory experimental program aimed at better understanding the scour around and burial of heavy cylindrical objects under oscillating flow on a sandy bed are described. This study was motivated by its application to the dynamics of isolated cobbles/mines on a sandy floor under nonlinear progressive waves, such as that occur in shallow coastal waters beyond the wave-breaking region. In the experiments, nonlinear progressive waves were generated in a long wave tank of rectangular cross-section with a bottom slope. Model mines (short cylinders) were placed on the sandy bottom and the temporal evolution of the bed profile and the velocity field in the near field of the object were observed. Experiments were conducted at relatively high Reynolds numbers for a range of flow conditions, which can be characterized by the Keulegan–Carpenter number and Shields parameter. Depending on the values of these parameters, four different scour regimes around the cylinder including periodical burial of cylinder under migrating sand ripples were observed; they were classified as: (i) no scour/burial, (ii) initial scour, (iii) expanded scour, and (iv) periodic burial cases. A scour regime diagram was developed and the demarcation criteria between different regimes were deduced. Semi-empirical formulae that permit estimation of the scour depth with time, the equilibrium maximum scour depth and length, and conditions necessary for the burial of the cylinder as a function of main external parameters are also proposed.

© 2003 Elsevier Science Ltd. All rights reserved.

*Keywords:* Sand ripples; Short cylinder; Scour; Burial; Shoaling waves

---

\* Corresponding author. Tel.: +1-480-935-8746; fax: +1-480-965-8746.

*E-mail address:* [s.voropayev@asu.edu](mailto:s.voropayev@asu.edu) (S.I. Voropayev).

<sup>1</sup> Also at: Institute of Oceanology, Russian Academy of Sciences, Moscow 117851, Russia.

## 1. Introduction

In this communication, we present results on the scour around and subsequent burial of relatively short horizontal cylinders placed on a sandy slope under nonlinear progressive waves. This research was motivated by recent naval interests on the behavior and possible burial of large cylindrical objects (mines) in coastal environments where nonlinear waves play the dominant role. The problem of the fate of 3D objects (e.g. relatively short horizontal cylinder) in shoaling zone has not been studied previously, and the present work constitutes an investigation in this context.

When heavy solid objects such as pipelines, piles, etc., are placed on a sandy seabed, the flow near the bed is modified by the solid object. Usually the velocity near the object increases, and as a result the *local* Shields parameter also increases leading to a significant increase of the local sediment transport rate. Consequently, the bottom topography in the vicinity of the solid object changes from the previous equilibrium (or quasi-equilibrium) state, and noticeable scour around the object may be observed. Given its importance in understanding the stability of coastal structures exposed to the scour/burial, many studies have been conducted on the mechanisms and dynamics of scour and scour patterns around different objects (see, e.g. Herbich et al., 1984 and recent review paper by Sumer et al., 2001). Theoretical modeling of this strongly nonlinear and complicated problem is still in infancy, and only initial dynamics of ripple formation has been analyzed quantitatively in the linear and weakly nonlinear limits for the case of the formation of rolling grain ripples on an initially flat sandy bed (Blondeaux et al., 2000; Vittory and Blondeaux, 1990). There are also not many numerical simulations on the problem either, mainly due to the difficulty of parameterizing the bed and suspended sediment transport rates in the continuity equation for sediments. In spite of this and other difficulties, satisfactory predictions have been achieved recently for simplified situation of a vertical cylinder in a mean flow (Kan et al., 2001; Roulund et al., 1998). Since strong simplifications are used in theoretical and numerical approaches, the results obtained require experimental verification, which mainly comes from laboratory experiments. In this regard, traditionally, more attention has been focused on steady-currents past two-dimensional objects due to its immediate applications to scour at bridge piers in rivers (Sumer et al., 2001). A more complicated situation is the scour problems in coastal and offshore engineering, where waves are the dominating factor, and this topic have received lesser attention. Since objects of interest in wave-induced scour studies are two-dimensional, for example pipelines (long horizontal cylinders) and vertical piles (mostly long vertical cylinders), significant progress has been achieved in studying two-dimensional flow and scour dynamics around solid objects. The mechanism of scour has been clarified (see e.g. Cevik and Yuksel, 1999; Sumer et al., 1992) allowing a better understanding and predictive capability for assessing scour at two-dimensional coastal structures. The case of short horizontal cylinders, where the flow is essentially three-dimensional, has not been studied previously.

In Section 2, we present a simple scaling framework on which the scour around a three-dimensional object placed on a movable bed under wave forcing can be analyzed. Experimental set-up and flow conditions are described in Section 3. The

results of experiments conducted are presented in Section 4, and the main conclusions are given in Section 5.

## 2. General analysis

Consider a heavy cylinder of diameter  $D$  and length  $L$  placed at time  $t = 0$  on a layer of sand with the grain size  $d$  and density  $\rho_s$  in horizontally oscillating water flow. The far-field maximum horizontal water velocity in the area of interest is  $U$  and the oscillating frequency is  $\omega$  (period  $T = 2\pi/\omega$ ). The water density is  $\rho$  and kinematic viscosity is  $\nu$ . In general, the cylinder axis is not parallel to the wave front direction and has an angle  $\theta$  relative to it. Taking into account that the gravitational acceleration,  $g$ , plays an important role in the sediment transport,  $g$  should also be included in the set of external parameters. Suppose that the cylinder is sufficiently heavy and does not move under the wave action; thus the cylinder density is unimportant. Then, for oscillations under linear waves (where the amplitude of the horizontal water particle excursion,  $\epsilon$ , may be simply estimated as  $\epsilon = U/\omega$ ), the full set of the primary external parameters determining the scour/burial characteristic, say  $A$ , of the cylinder is given by

$$A = F(D, L, d, \rho_s, t, U, \omega, \rho, \nu, g, \theta), \quad (1)$$

where  $F$  is a function. [For nonlinear waves,  $\epsilon$  needs to be measured directly, as discussed in Section 3.2, or calculated numerically (Grilli et al., 2003).] Four of these 11 external parameters in Eq. (1) have independent dimensions, leading to seven dimensionless governing parameters. These can be rationally chosen using some additional physical arguments, relevant to the problem considered.

First, it is clear that parameters  $\rho_s$ ,  $\rho$  and  $g$  are important only in a combination  $g^* = g(s-1) = g(\rho_s/\rho-1)$ , which is the reduced gravity force. This gives

$$A = F(D, L, d, t, U, \omega, \nu, g^*, \theta). \quad (2)$$

Second, standard physical arguments and consideration of the bottom boundary layer and forces acting on the cylinder and sand particles lead to the following six-dimensional parameters, which govern the scour process: cylinder Reynolds number,  $Re = DU/\nu$ ; Keulegan–Carpenter number,  $KC = 2\pi U/D\omega = UT/D = 2\pi\epsilon/D$ ; Shields parameter,  $Sh = U^{*2}/g^*d = U^2f/2g(s-1)d$ ; non-dimensional time,  $\tau = \omega t$ ; cylinder aspect ratio,  $a = D/L$ ; and cylinder orientation angle,  $\theta$ . Here  $U^* = U(f/2)^{1/2}$  is the friction velocity, and  $f$  is the friction coefficient. In a laminar regime  $f = C/Re_0$ , where  $Re_0 = \delta U/\nu = 2^{1/2}U/(\nu\omega)^{1/2}$  is the boundary layer Reynolds number and  $\delta = (2\nu/\omega)^{1/2}$  is the boundary layer thickness. For a smooth bottom, the value of  $C$  may be calculated as  $C = 2^{3/2}$  (Nielsen, 1992; Sleath, 1984). In our experiments,  $Re_0 \approx 200$ , the bottom is not smooth with a typical ratio of  $U/\omega d \approx 150$ . The estimated roughness Reynolds number,  $Re^* = U^*k/\nu$  ( $k = 2.5d$  is the roughness height) is larger than 30, and hence the flow near the bed is turbulent. Also the dimensionless grain size,  $d^* = [g^*d^3/\nu^2]^{1/3} \approx 15$ , and hence the grain movement at the bed is expected to be largely independent on viscous effects (Hager and Del Giudice, 2001).

Under these conditions, a well-established formula for  $f$  may be used (Nielsen, 1992; Sleath, 1984)

$$f = 0.00251 \exp\{5.21(k/\varepsilon)^{0.19}\}. \quad (3)$$

Thus, any dimensionless scour/burial characteristic, say  $B$ , is a function of six dimensionless parameters

$$B = \Phi(Re, KC, Sh, \tau, a, \theta). \quad (4)$$

The dependence (4) is still too intricate for a systematic experimental study. For simplicity, as a first step, we consider below experimentally the steady or quasi-steady state,  $\tau \gg 1$ , with  $a = \text{const}$  ( $= 5$ ) and  $\theta = \text{const}$  ( $= 0$ , cylinder axis is parallel to the wave front). Also suppose that  $Re$  is large enough (see Table 1) for the processes to be independent on  $Re$  (complete similarity). After such simplifications, Eq. (4) becomes

$$B = \Phi(KC, Sh). \quad (5)$$

Below, based on experimental results, the form of Eq. (5) is delineated for main scour/burial characteristics, which include the scour/burial regime diagram and equilibrium depth and length of scour. After that, the time evolution of scour depth on dimensionless time,  $\tau$ , is considered.

### 3. Experimental set-up and flow conditions

#### 3.1. Experimental set-up

A detailed description of the experimental facility can be found in Voropayev et al. (2001) and only a brief description is given subsequently. A large glass-walled wave tank ( $32 \times 0.9 \times 1.8 \text{ m}^3$ ) with a slopping bottom was used in the experiments to generate progressive waves. The tank is filled with tap water (density  $\rho = 1 \text{ g cm}^{-3}$ , viscosity  $\nu = 10^{-2} \text{ cm}^2 \text{ s}^{-1}$ ) to a depth of  $H_0 = 105 \text{ cm}$  near the wave paddle

Table 1  
Typical values of parameters

	Laboratory	Ocean
$U$ ( $\text{cm s}^{-1}$ )	10–46	50
$T = 2\pi/\omega$ (s)	2.5–5	10
$D$ (cm)	2.8–8	60
$d$ (cm)	0.06	0.1
$KC$	6–60	10
$Sh$	0.015–0.27	0.1
$Re$	4000–35,000	300,000

where the tank bottom is horizontal (see schematic in Fig. 1). The tank consists of a number of sections, which are numbered 0–47, with the section 0 being the panel to the left of the wave-maker and each section is 61 cm in length. A vertical paddle driven by a piston, installed at one end of the tank, is used to generate sinusoidal periodic waves of frequencies  $\omega = 2\pi(0.2\text{--}0.4 \text{ Hz}) \text{ s}^{-1}$  and peak-to-peak displacement of the paddle motion of  $2\epsilon_0 = 10\text{--}25 \text{ cm}$ . A layer of quartz sand (mean grain size  $d = 0.06 \text{ cm}$ , density  $\rho_s = 2.6 \text{ g cm}^{-3}$ ) of thickness 20 cm was placed on the wooden bottom with a slope of 1:24 (length 26 m). The horizontal and vertical velocity components were measured at different positions (sections) along the slope using a standard three-component acoustic Doppler velocimeter (ADV) (Snyder and Castro, 1999). The ADV probe, which is attached to a long supporting rod, is fixed to a carriage. To obtain representative data, the velocity records were phase averaged for a time interval of 40 oscillation periods. The carriage is mounted on rails on the top of the tank and has three degrees of freedom, movement along the tank as well as transverse and vertical directions.

Before each experiment the sand at the slope was leveled and made flat. The tank was then filled with water, and the object was placed at the bottom in a chosen tank section under the carriage. In most experiments short heavy cylinders of different diameter  $D$  ( $= 2.8\text{--}8 \text{ cm}$ ) and length  $L$  with an aspect ratio of  $a = L/D = 5$  were used. In one case, for comparison, long cylinder with  $a = 15$  was also used. Cylinders are made from solid aluminum or plastic (filled with sand) and have a density of either  $2.7$  or  $1.9 \text{ g cm}^{-3}$ ; they are heavy enough not to move under the wave action.

Information on bottom topography was obtained using two Super VHS video cameras attached to the carriage. One camera is fixed at the top and the other at a side of the carriage at the level near the tank bottom, thus giving top and side views of the scour patterns. After the experiment, video records were analyzed, and data on topography changes with time (e.g. scour) were obtained.

In selected runs the scour depth was measured directly using the so-called ‘structured light’ method, a rather accurate ( $\pm 0.1 \text{ cm}$ ) method proposed by Faraci et al.

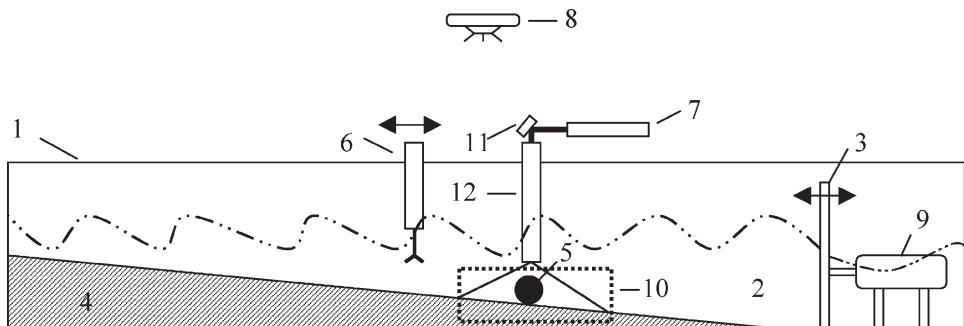


Fig. 1. Schematic of the experimental system: 1. tank; 2. water; 3. vertical wave-maker ( $\omega$ , frequency;  $\epsilon_0$ , amplitude of horizontal displacement); 4. sloping bottom (slope = 1/24); 5. cylinder; 6. ADV attached to carriage; 7. laser; 8. photo or digital video camera; 9. hydraulic system to move wave-maker; 10. view frame of a digital camera which is connected to a computer; 11. mirror; 12. light guide with splitting optics under the water level.

(2000). Therein, a narrow (thickness 0.1–0.2 cm) vertical laser sheet entering from the top illuminates the bottom and produces a bright line along the tank axis at the bottom (see schematic in Fig. 1). When viewing from the side through glass walls of the tank, this light line is straight when the bottom is flat, or curved for an undulating bottom, and its curvature is directly related to the sand surface elevation. Using high-resolution digital camera (model PIVCAM 10-30) placed obliquely to the horizon, this line was photographed periodically through the sidewalls. This oblique angle (usually 30–35°) should be sufficiently large to see the maximum scour, but not too large to compromise the accuracy of measurements. Using commercial software (TSI-Insight), the images of the line at the bottom were transformed into the surface elevations using scaling factors in horizontal ( $x$ ) and vertical ( $z$ ) directions. The scaling factors were determined prior to each run by photographing a calibrating grid, which was placed vertically at the bottom near the cylinder. To avoid undesirable reflections and scatter of the laser light sheet from the wavy water surface, a simple device was used. The optics (cylindrical lens, etc.) that was used to produce light sheet was installed under the water surface at the end of a rigid submerged hermetic tube containing air. The laser beam passed through this tube vertically to the splitter, without subjecting to surface waves under wavy surface. To minimize the interference of the vertical tube (diameter 2 cm), the tube was installed within a thin Plexiglas airfoil.

### 3.2. Background flow characteristics

Although the wave-maker forcing is purely sinusoidal, as the waves steepen and change the height along the propagation path, the underlying velocity profiles become increasingly nonlinear. At present there are no reliable theories to accurately calculate such nonlinear behavior, and hence one has to resort to sophisticated numerical simulations (see, e.g. Grilli and Horillo, 1997; Grilli et al., 1997). These simulations, however, require detailed verifications using experimental data (see Grilli et al., 2003). Since information on wave induced water motion is imperative for the interpretation of observations, in the present study the velocities under the waves were measured directly by using an ADV probe. To this end, waves were generated with a chosen frequency  $\omega$  [ $= 2\pi(0.2\text{--}0.4 \text{ Hz}) \text{ s}^{-1}$ ] and a paddle displacement amplitude  $\varepsilon_0$  ( $= 5\text{--}12.5 \text{ cm}$ ) in a water of fixed depth  $H_0$  ( $= 105 \text{ cm}$  near the wave-maker). The ADV data (sampling frequency 24 Hz) on the horizontal velocity were taken at the standard depth of 10 cm above the bottom at different sections along the slope after the flow was established. These data were averaged over 40 oscillation periods and the far-field maximum horizontal water velocity  $U$ , which is used as a primary external parameter in (1), was determined. By integrating the averaged velocity records over the time, the real amplitudes of the horizontal water particle displacement,  $\varepsilon$ , were obtained and then used to calculate the values of  $KC = 2\pi\varepsilon/D$  (thus avoiding the use of linear theory estimate  $\varepsilon = U/\omega$ ).

Typical time records for three velocity components,  $u$ ,  $v$ ,  $w$ , as measured by the ADV probe at 10 cm above the bottom, are given in Fig. 2. All data are taken in the undisturbed flow (without the cylinder) and phase averaged over 40 wave periods.

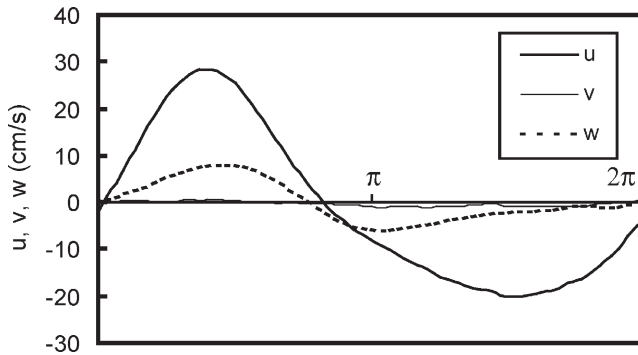


Fig. 2. Horizontal  $u$ ; transverse  $v$ ; and vertical  $w$ ; flow velocity components measured at 10 cm above the bottom by the ADV probe in section 23. The data are phase averaged over 40 wave periods. Experimental conditions are:  $\omega = 0.4$  Hz,  $\varepsilon_0 = 5$  cm,  $U = 28$  cm s<sup>-1</sup>, and  $\varepsilon = 9.7$  cm.

As can be seen from the figure, the transverse velocity component,  $v$ , is practically negligible yielding a two-dimensional flow field in the wave tank. The vertical velocity component,  $w$ , is much smaller than the horizontal one,  $u$ . It rapidly decreases with the depth and tends to be zero at the bottom. The horizontal velocity,  $u$ , does not change significantly with the depth, except in the bottom boundary layer. For relatively large waves,  $u$  is asymmetric and nonlinear. In this example the wave-maker oscillates sinusoidally with the horizontal amplitude  $\varepsilon_0 = 5$  cm, but the observed amplitude,  $\varepsilon$  of the horizontal water particle displacements increases along the slope and becomes equal to  $\varepsilon = 9.7$  cm in section 23. For clarity the velocity components are shifted to the same phase in Fig. 2.

In Fig. 3, typical horizontal along slope velocities  $u$  are shown for three different experimental conditions. These phase-averaged data show the effects of the wave frequency and position along the slope on the maximum horizontal along slope velo-

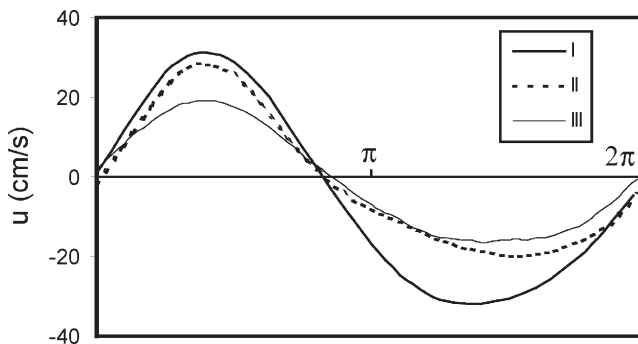


Fig. 3. Typical examples of the horizontal velocity component  $u$ , measured at standard depth (10 cm from the bottom) for different flow conditions. The data are phase averaged over 40 wave periods. Experimental parameters are:  $\omega = 0.6$  Hz,  $\varepsilon_0 = 5$  cm,  $U = 32$  cm s<sup>-1</sup>,  $\varepsilon = 6.7$  cm, section 23 (I), 0.4 Hz, 5 cm, 28 cm s<sup>-1</sup>, 9.7 cm, 23 (II), 0.4 Hz, 5 cm, 19 cm s<sup>-1</sup>, 6.5 cm, 14 (III).

city,  $U$ , and the amplitude  $\epsilon$  of the horizontal water particle displacements. Similar data were taken prior to each experiment, from which  $U$  and  $\epsilon$  were obtained for interpretation of results.

## 4. Experimental results

In total 31 experiments were conducted, and the range of primary dimensional parameters and main dimensionless governing parameters used in the experiments are given in Table 1. Also included are the typical values for ocean mine burial situations.

As can be seen from Table 1, in the experiments, two main dimensionless parameters,  $KC$  and  $Sh$ , match rather satisfactorily with the typical oceanic values. Large oceanic Reynolds numbers cannot be matched correctly in the experiments, but their laboratory values are rather high to justify the Reynolds number similarity assumption made in Section 2.

### 4.1. General description and classification

In our experiments, depending on the values of main governing parameters, the acceleration of flow around cylinders led to different types of local scour and bottom boundary/cylinder interactions. The results of steady or quasi-steady scour/burial processes are considered in this section, and Sections 4.2 and 4.3. The time dependent processes are considered later in Section 4.4.

Before discussing scour/burial scenarios observed at large times, it is useful to present a qualitative description of flow around short horizontal cylinder on a solid bed in oscillatory flow. [As mentioned, to our knowledge no data exists in open literature on this topic, although numerous studies have been conducted using long cylinders including oscillatory flow around free horizontal cylinder (Sarpkaya, 1986, 2002) and vertical cylinders on a solid bed (Faraci et al., 2000; Sumer et al., 1997) (see also the book by Zdravkovich, 1997).]

The results of visual observations are summarized schematically in Fig. 4, where the formation of two energetic tip vortices near the ends of a finite-length cylinder and a central vortex near its center, during the onshore water motion, are shown. Tip vortices have an approximately vertical axis of rotation and they are counter rotating. In the central vortex the water moves along the cylinder surface, the axis of vortex being approximately horizontal. These three vortices are rather energetic and form periodically at each phase of the flow. Because of the asymmetry of the flow field (due to the waves nonlinearity), however, the vortices generated in the onshore phase of the flow are usually more energetic than those generated during the offshore phase of the flow. Those vortices are the main driving force for the sediment transport and scour around the cylinder. The flow near the cylinder is strongly three-dimensional and its structure changes depending on the relative intensities of tip and central vortices. Detailed data on various flow regimes that occur in different external parameters ranges are of definite interest, and obtaining such

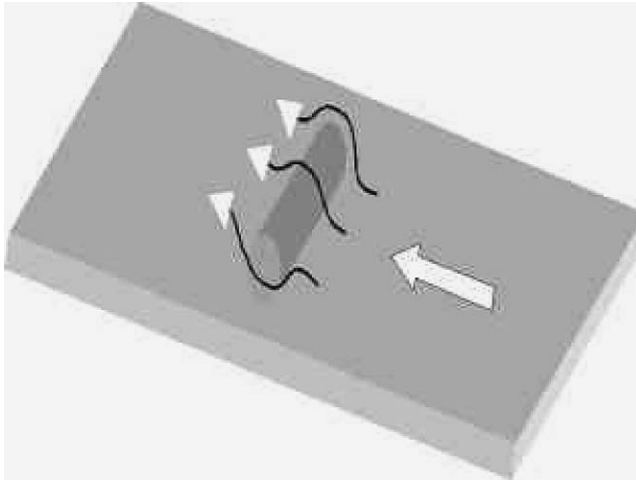


Fig. 4. Schematic showing the formation of energetic tip vortices (near the ends of a finite-length cylinder) and central vortex (near the center of the cylinder) during the onshore water motion (direction of water motion is shown by a large arrow and of vortices are shown by small arrows).

data is the focus of an ongoing laboratory study. For the purpose of the current study, however, simplified flow description given above is sufficient.

In the experiments, depending on the governing parameter ranges, four main types (I–IV) of near-field bed evolutions can be classified: I, no scour; II, initial scour; III, expanded scour; and IV, periodic burial of the cylinder. Some details of these cases are discussed subsequently.

*No scour (regime I).* This regime occurs when the local flow velocity is less than the critical velocity for the initiation of sediment motion. In this regime, the near-field flow is not energetic enough to cause any noticeable scour, and this regime persists for fixed experimental conditions.

*Initial scour (regime II).* The typical scour pattern for this regime is shown in Fig. 5 for two different times. As can be seen, a symmetric scour with respect to longitudinal (along slope) axis passing through the center of the cylinder is formed around the cylinder. This scour pattern consists of a central gap near the center of the cylinder (A) and two additional gaps (B) at the tips of the cylinder. In most experiments, this scour pattern was observed mainly in the onshore side of the cylinder due to the nonlinearity of the waves; however, for weakly nonlinear waves, similar, but less intensive, scour pattern could also be formed on the offshore side of the cylinder. Although the local scour pattern formed does not change significantly with time, at larger times, small sand waves are generated at the tips of the cylinder (Fig. 5(a)), spread and initiate ripple formation in the onshore direction (Fig. 5(b)). These ripples are relatively small and rapidly decay away from the cylinder, and they exist only because of vortices.

To show the importance of tip vortices in the scour, an example of scour pattern around a long cylinder is given in Fig. 6. This cylinder spans practically the entire

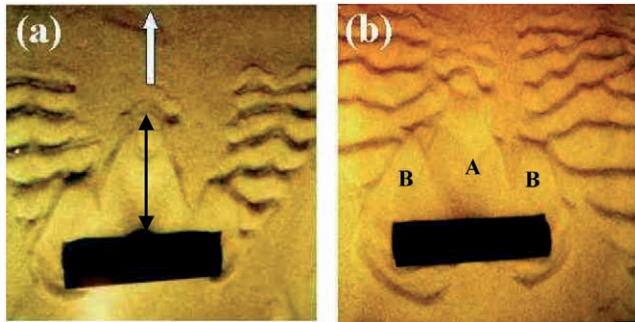


Fig. 5. Photographs showing the top view of the initial scour patterns (regime II) around a cylinder. White arrow shows the onshore direction, black arrow shows the maximum equilibrium scour length,  $L^*$ . Time  $t = 120$  (a), 220 (b) minutes after the initiation of wave forcing; A. central scour gap. B. Tip scour gap. Experimental parameters are:  $D = 8$  cm,  $\omega = 0.2$  Hz,  $U = 25$  cm  $s^{-1}$ ,  $\varepsilon = 12$  cm,  $KC = 10$  and  $Sh = 0.082$ . For the sake of better lighting, these photographs were taken at an angle to the vertical leaning toward onshore direction. As a result the cylinder looks slightly tilted and scour length looks shorter than the real length ( $L^* = 27$  cm) while the cylinder diameter remains the same.



Fig. 6. An example showing typical scour pattern surrounding a long cylinder. Experimental parameters:  $D = 4$  cm,  $KC = 20$ ,  $Sh = 0.07$ , sand accumulation can be seen on the onshore side of the cylinder. Time  $t = 320$  min. The onshore direction is to the left. Horizontal line shows the initial bed level.

width of the tank and there are no noticeable tip vortices near its ends. The flow around the cylinder is approximately two-dimensional and sand is simply accumulated uniformly along the cylinder in this regime.

Once formed, the initial scour, similar to that shown in Fig. 5, can either persist many hours without any noticeable changes or transform into other regimes depending on the values of the governing parameters (see the scour regime diagram in Fig. 12 to be discussed later).

*Expanded scour (regime III).* When the water motion is more energetic than in the previous case and flow conditions are suitable for inducing natural ripples, the scour initially develops as in regime (II) but then becomes unstable and transforms into an expanded scour regime, as follows.

As soon as the waves are initiated, ‘the initial scour’ (regime II) begins to form around the cylinder. At the same time, ripples start forming close to the wave breaking point where the flow is energetic and the Shields parameter is rather high. These ripples propagate in the offshore direction into deep water and soon reach the cylinder. [Detailed data on the ripple formation and dynamics of ripple front propagation are reported in Voropayev et al. (2002).] When the ripples reach the cylinder, the tip scour gaps of the initial scour merge with the central gap forming a semi-elliptical scour pattern onshore of the cylinders (see the schematic in Fig. 7). This transformation of initial scour (regime II) to an expanded scour (regime III) occurs only when the ripple height,  $h$ , is not large enough and less than the diameter of the cylinder ( $D/h > 1$ ).

As long as  $D > h$ , the flow disturbances caused by the cylinder is dominant, and expanded scour pattern is stable and persists for many hours. However, in the opposite case of  $D < h$ , the ripple effects become dominant and this scour pattern transforms into a case of periodic burial (see regime IV).

A close view of an expanded scour pattern is shown in Fig. 8. This photograph clearly indicates the difference between the ripple height and the cylinder diameter ( $D/h > 1$ ). The scour width and depth are not very well visible in this photograph, but are more clearly visible in the photograph of Fig. 9 based on the ‘structured light’ technique. The bright line shows the intersection of the vertical laser light sheet with the sand bottom, and the curvature of this line gives information on the depth of scour. These two photographs (Figs. 8 and 9) were taken in the same experiment and approximately at the same time. In this particular experiment, the maximum scour depth,  $S^*$ , is approximately  $1.2D$ . The expanded scour pattern can be stable (regime III) or may transform into periodic burial (regime IV) depending on flow conditions.

*Periodic burial (regime IV)*. This regime mostly occurs when the flow is very energetic and when the ripple heights are comparable or larger than the cylinder diameter ( $h/D > 1$ ). The scour develops first, as in regime (II), and it remains in this regime until ripples arrive from the onshore direction and expanded scour

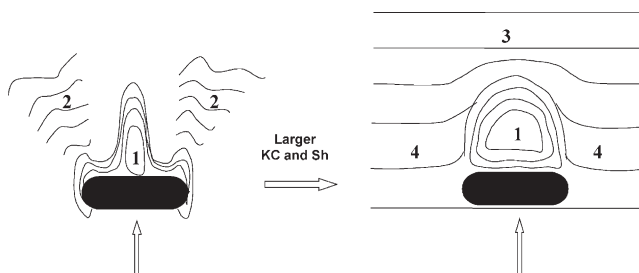


Fig. 7. A schematic of the transformation of initial scour pattern (regime II) to the expanded scour (regime III) for large values of the Keulegan–Carpenter number and Shields parameter when diameter of the cylinder is larger than the ripple height ( $D/h > 1$ ). Vertical arrows show the onshore direction. (1) central gap, (2) small sand waves generated near cylinder tips and propagating under approximately  $35\text{--}45^\circ$  from the cylinder, (3) undisturbed incoming ripples, and (4) ripples around the scour gap.



Fig. 8. A photograph showing an oblique view of the expanded scour pattern (regime III) around a cylinder. The onshore direction is to the left. Time  $t = 78$  min after the initiation of wave forcing. Experimental parameters:  $D = 8$  cm,  $\omega = 0.4$  Hz,  $\varepsilon = 11.7$  cm,  $U = 45.7$  cm s<sup>-1</sup>,  $KC = 10$ ,  $Sh = 0.27$ .

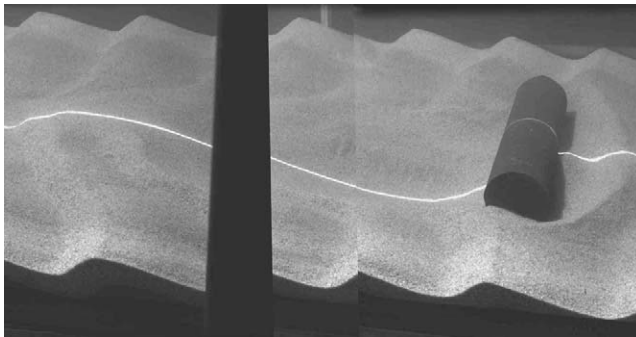


Fig. 9. A photograph showing an oblique view of the expanded scour pattern (regime III) around a cylinder. The onshore direction is to the left. Bright line shows the intersection of a vertical laser sheet with the sand bottom and its curvature gives information on the depth of the scour. Experimental parameters (including time) are the same as in Fig. 8.

(regime III) appears. The ripples arriving first are relatively small, but with time their size increases and soon reaches equilibrium state. When ripples increase in size, expanded scour becomes unstable and transforms into periodic burial regime, a typical example of which is shown in Fig. 10. The main mechanism here is the ripple migration that takes place under progressive waves. Scour due to the presence of the cylinder is significantly suppressed by the ripples activity in this case. When the cylinder is under a ripple crest and  $h/D > 1$  (Fig. 10(a)), the cylinder is completely buried and there is no scour. Whence the ripple crest overruns the cylinder, however, the upper part of the cylinder is exposed out of the sand and an elliptical scour gap (similar in shape to, but less pronounced than, that observed in the expanded scour regime) starts to develop in the onshore direction. The partly exposed cylinder

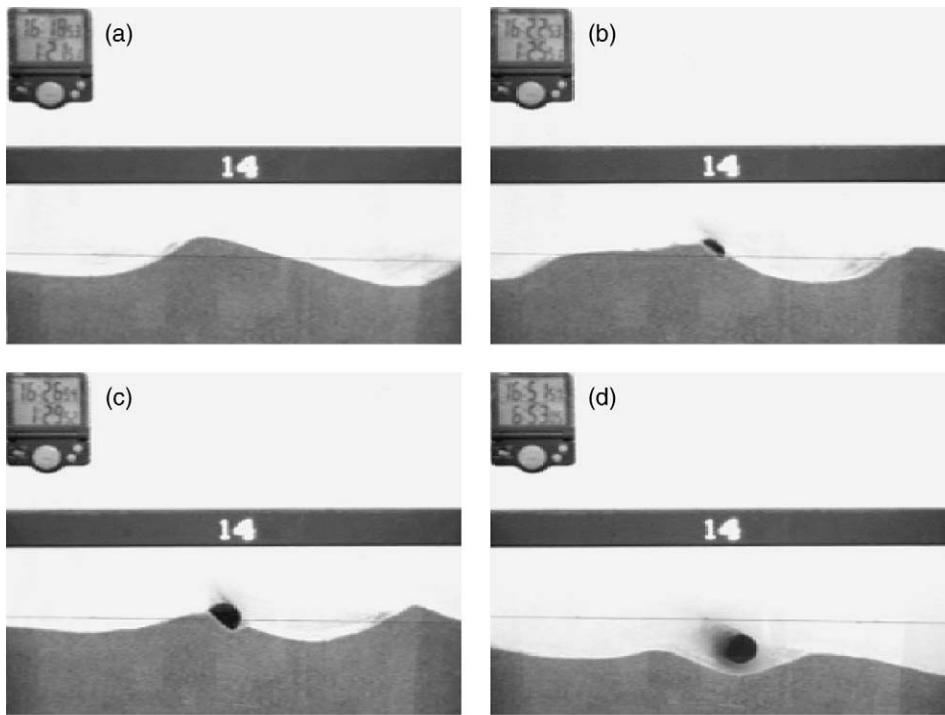


Fig. 10. Periodic burial of a cylinder under large migrating ripples at relatively high values of  $KC = 38$  and  $Sh = 0.1$ . Time  $t = 81$  (a), 85 (b), 89 (c) and 413 min (d). Typical period of burial is approximately 22 min and the last frame (d) was taken after 14.5 burial periods. When the ripple size is comparable to the cylinder diameter, the cylinder is overrun by migrating ripples and it is buried periodically. Ripples drift in the onshore direction (to the left). The faded line represents the initial bed.

initiates scour and modifies (or destroys) the nearest ripple crest that has already passed over the cylinder (Fig. 10(b)). Thereafter the cylinder is sited in the ripple trough and, depending on  $h/D$ , it may be completely (Fig. 10(c)) or partly recovered from the sand. This quasi-steady process repeats itself with time (Fig. 10(d)).

For complete burial to occur, ripples should reach their equilibrium (mature) size. At the earlier stages of the periodic burial, therefore, only partial periodic burial takes place. Later the size of the oncoming ripples increases, so as the tendency for complete burial.

#### 4.2. Scour/burial regime diagram

Here a regime diagram is presented on the Keulegan–Carpenter ( $KC$ ) and Shields ( $Sh$ ) parameter space to map the regimes observed above. Beforehand, it is useful to make some estimates that will aid clarify this regime diagram. Given the complexity of the flow and unavailability of a theoretical foundation, only empirical approaches will be used to obtain such estimates.

Consider the regime I. One may expect that there will be no scour if the *local* (near the cylinder) Shields parameter is less than a critical value,  $Sh^*$  necessary for the initiation of sediment motion. For undisturbed oscillatory flow (no objects at the bottom) this critical value can be taken as  $Sh_1 \approx 0.04$  (see, e.g. Sleath, 1984). In the vicinity of a three-dimensional body (e.g. near tips of a short cylinder) the maximum *local* flow velocity exceeds the undisturbed value,  $U$ , by a factor 1.5 (Batchelor, 1967). This gives the estimate  $Sh^* \approx Sh_1 / 1.5^2 \approx 0.018$ . In addition, it is also clear that there will be no significant scour when vortices shown schematically in Fig. 4 are sufficiently weak or absent. General condition for the generation of such vortices for impulsively started flow around a cylinder is found in Van Dyke (1973) as  $2\varepsilon / D \approx 0.65$ . This gives the estimate  $KC^* \approx 2$ . Thus, in a simplified flow regime diagram (Fig. 11), regime (I) is expected when

$$KC < KC^* \approx 2 \quad \text{or} \quad Sh < Sh^* \approx 0.018. \tag{6}$$

Now consider regime (IV), wherein the ripples formed away from the body are important. The critical value of the Shields parameter for the initiation of ripple formation can be estimated as  $Sh^{**} \approx 1.16^2 Sh_1 \approx 0.054$  (Sleath, 1984). The ripples become dominant when  $D/h < 1$ . Here  $h$  is the mature ripple height, and  $h$  may be estimated by the empirical formulae of Nielsen (1992) and Sleath (1984):  $h \approx 0.2 L$ ,  $L \approx 2.2 \varepsilon^*$  ( $L$  is the ripple length,  $\varepsilon^*$  is the critical value of  $\varepsilon$  for given  $D$ ). From here it follows:  $KC^{**} = 2\pi\varepsilon^* / D \approx 14$  is the critical value of the Keulegan–Carpenter number, above which periodical burial under migrating ripples occurs, or the conditions for regime (IV), viz.

$$KC > KC^{**} \approx 14, \quad Sh > Sh^{**} \approx 0.054. \tag{7}$$

For regime (III), the formation of ripples is important but they play secondary role and have relatively small size,  $D/h > 1$ . Reasoning as above shows that regime (III) will be realized at approximate asymptotic conditions

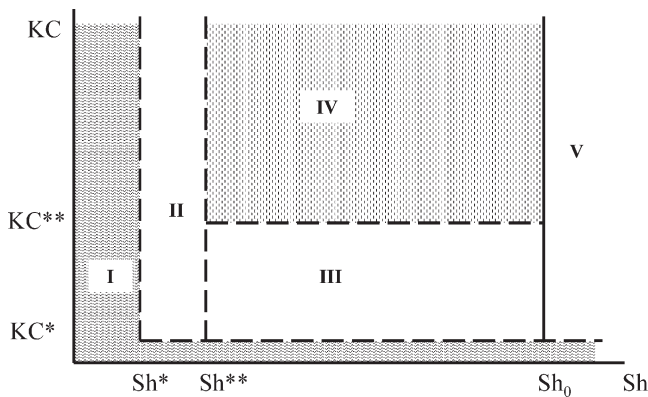


Fig. 11. Simplified estimated asymptotic scour/burial  $KC$ – $Sh$  regime diagram. (I) No scour regime, (II) initial scour regime, (III) expanded scour regime, (IV) complete/partial periodic burial regime, and (V) sheet flow regime. The estimated values for  $KC^*$ ,  $KC^{**}$ ,  $Sh^*$ ,  $Sh^{**}$  and  $Sh_0$  are given in Eqs. (6) and (7).

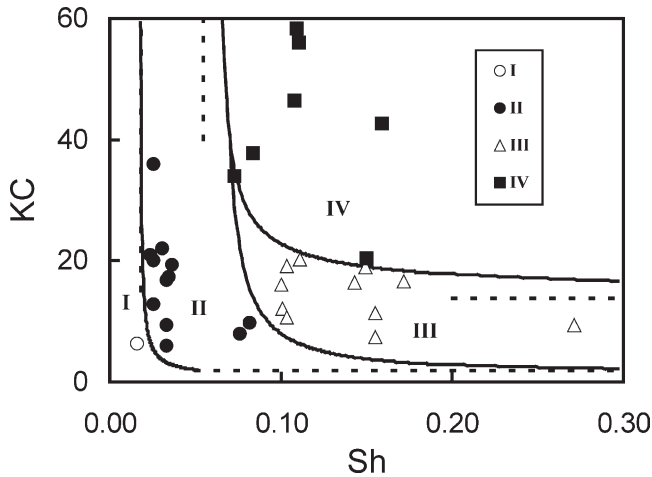


Fig. 12. Experimental diagram showing four different regimes (I–IV) for cylinder scour/burial depending on the values of  $KC$  and  $Sh$  parameters. Three solid lines show transition curves (boundaries) between four basic regimes. Analytical parameterizations for transition curves are given by Eqs. (9)–(11). Dashed lines show the estimated limiting asymptotes for different regimes.

$$KC^* < KC < KC^{**} \approx 14, \quad Sh > Sh^{**} \approx 0.054. \tag{8}$$

At very high values of  $Sh$  ( $> Sh_0 \approx 0.83$ ), all bottom topography is ‘washed’ away and a ‘sheet’ flow regime (V) is realized; this regime, however, was unattainable in the present experiments. Collectively, the above estimates are depicted on the simplified asymptotic regime diagram shown in Fig. 11.

The results of all experiments (see Table 1) are summarized in the experimental regime diagram shown in Fig. 12. Based on the observations, the experiments were categorized into four different quasi-equilibrium scour regimes (I–IV) and are depicted by different symbols. Dashed lines show the asymptotic estimates of Fig. 11. Three solid lines show the transition curves (boundaries) between four basic regimes, identified numerically by trial and error, and the following simple parameterizations were chosen. The solid curve separating regimes (I) and (II) is given by

$$KC = KC^* + (Sh^{**} - Sh) / (Sh - Sh^*). \tag{9}$$

For the curve separating the regimes (II) and (III)

$$KC = KC^* + (Sh_0 - Sh)^5 / (Sh - Sh^{**}), \tag{10}$$

and the curve separating the regimes (III) and (IV) is

$$KC = KC^{**} + 1 / (Sh - Sh^{**})^{2/3}. \tag{11}$$

Here  $Sh^* \approx 0.018$ ,  $Sh^{**} \approx 0.054$ ,  $Sh_0 \approx 0.83$ ,  $KC^* \approx 2$ , and  $KC^{**} \approx 14$ .

The above parameterizations (9)–(11) are purely empirical and lack physical or theoretical underpinning. They, however, are the simplest, give the best-fit to the experimental data and correctly reproduce the limiting asymptotic behaviors.

#### 4.3. Equilibrium scour dimensions as functions of $KC$ and $Sh$

In selected experiments the structured light technique was used and, in addition to visual observations, quantitative data on the scour depth,  $S$ , were obtained. Using these data, values of the maximum equilibrium scour depth,  $S^*$ , and scour length,  $L^*$ , in the central scour gap (see Fig. 5) were obtained for the initial scour (regime II). Preliminary observations demonstrated that dimensionless value of  $S^*/D$  strongly depends on both  $KC$  and  $Sh$ , while  $L^*/D$  depends mostly on  $KC$  only. The value of  $S^*/D$  increases when  $KC$  or  $Sh$  increases and  $L^*/D$  approximately linearly increases with  $KC$ . Before presenting the measurements, let us first return to Eq. (4) and attempt some preliminary estimates. Consider

$$S^*/D = F(KC, Sh). \quad (12)$$

Suppose that the rate of change of function  $F$  decreases exponentially with  $KC$  and  $Sh$  [which is typical of relaxation processes following the perturbations caused by external means or internal dynamical processes (see Voropayev et al., 1999)] when  $KC$  or  $Sh$  exceeds the critical values, say  $KC^* \approx 2$  and  $Sh^* \approx 0.018$ . This gives

$$\frac{F}{KC} \propto \exp\{-m(KC - KC^*)\}, \quad \frac{F}{Sh} \propto \exp\{-n(Sh - Sh^*)\}, \quad (13)$$

where  $m$  and  $n$  are constants. Integrating these differential equations, one has the following estimate

$$S^*/D = F(KC, Sh) = \text{const}[1 - \exp(-m(KC - KC^*))][1 - \exp(-n(Sh - Sh^*))], \quad (14)$$

where  $\text{const} = O(1)$  and  $m$  and  $n$  are empirical coefficients. Thus function (14) may be written as

$$S^*/D = \text{const}[1 - \exp(-m(KC - 2))][1 - \exp(-n(Sh - 0.018))]. \quad (15)$$

Using experimental results, the constants can be evaluated as  $\text{const} \approx 1.3$ ,  $m \approx 0.06$  and  $n \approx 40$ .

Comparison of measured,  $S^*/D$  (exp), and calculated,  $S^*/D$  (cal), (using 15) values of the maximum dimensionless scour depths for different Keulegan–Carpenter numbers,  $KC = 6–24$ , and Shields parameters,  $Sh = 0.026–0.15$ , for the initial scour regime (regime II) is given in Fig. 13. The proposed approximation (15) satisfactorily describes data from 11 experiments. Note that similar exponential dependencies on  $KC$  were successfully used by Sumer et al. (1992, 2001) to describe maximum scour depth around vertical cylinders. The dependence on  $Sh$  was not considered in those papers.

Experiments show that dimensionless maximum equilibrium scour length  $L^*/D$  in the central scour gap (see Fig. 5) depends mostly on one parameter  $KC$ , and  $L^*/D$  approximately linearly increases with  $KC$ . This gives

$$L^*/D = \text{const} * KC. \quad (16)$$

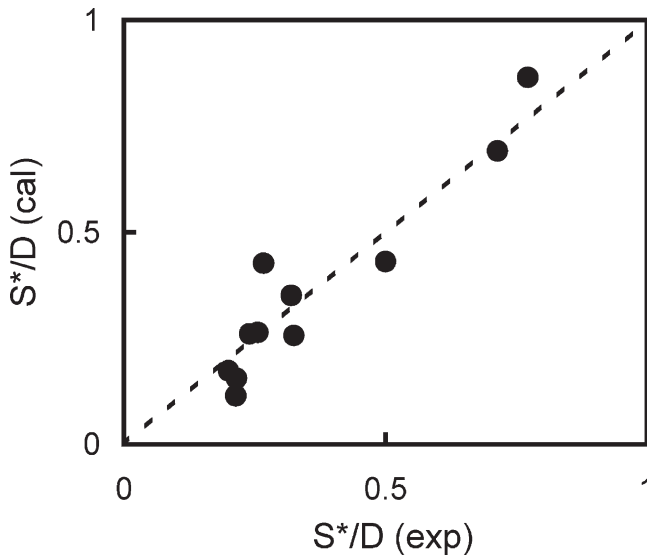


Fig. 13. Comparison of measured,  $S^*/D$  (exp), and calculated,  $S^*/D$  (cal) values of the maximum dimensionless scour depths for different Keulegan–Carpenter numbers,  $KC = 6$ – $24$ , and Shields parameters,  $Sh = 0.026$ – $0.15$  for regime (II). Calculations were done with  $const \approx 1.3$ ,  $m \approx 0.06$  and  $n \approx 40$ .

The value of  $const^*$  in Eq. (16) may be estimated as follows. The disturbance, which is mostly responsible for the central scour gap, is the central vortex (see Fig. 4). This vortex is transported by periodic flow and its maximum displacement,  $L^*$ , should be approximately equal to the horizontal excursion of water,  $2\epsilon$ . Direct comparison of Eq. (16) with the experiment (see Fig. 14) gives  $const^* = 0.35$  and this

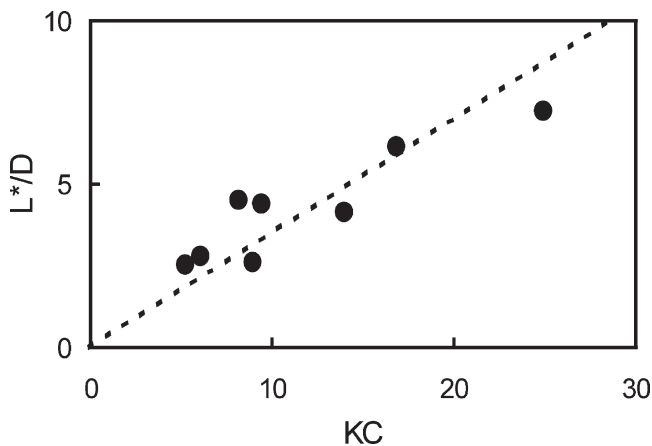


Fig. 14. Maximum dimensionless scour length,  $L^*/D$ , as a function of the Keulegan–Carpenter number,  $KC$  (for initial scour, regime II). Symbols show the results of measurements with  $D = 2.8, 5, 8$  cm and  $Sh = 0.036$ – $0.076$ . Dashed line shows the estimate  $L^*/D = 0.35 KC$  [see Eq (16)].

is equivalent to  $L^* = 2.2\varepsilon$ . It is interesting that with good accuracy  $L^*$  appeared to be equal to the typical length,  $L$ , of established vortex ripples, which can be estimated as  $L \approx 2.2\varepsilon$  (Sleath, 1984).

#### 4.4. Time dependence of the scour depth

This section considers the time dependence of scour. As soon as waves are initiated, scour around the cylinder takes place, which is rather fast at the beginning and slows down with time. After some characteristic time, the evolution of the scour pattern practically stops and an equilibrium scour pattern is established. Fig. 15 shows a typical series of photographs for the case of initial scour (regime II), taken during the use of the structured light technique. The light sheet was positioned at the center of the scour gap. There are no significant changes in the offshore side of the cylinder and only the onshore part of the scour is shown. The top of the cylinder is shown by an arrow in Fig. 15(a). As can be seen, fast changes occur in the first 15–25 min (Fig. 15(a,b)), and during,  $t = 25$ –100 min, scour gap increases rather slowly (Fig. 15(c)) and the scour gap practically does not change after  $t = 100$  min (Fig. 15(d)). Using such photographs, quantitative data on the scour depth as a function of time were obtained, as given in Fig. 16. Here we show a succession of seven scour profiles,  $S(x,t)$ , taken at different times in the same experiment as shown in Fig. 15. To show clearly the scour depth changes, different scaling is used in Fig. 16 in the horizontal,  $x$ , and vertical,  $S$ , directions and because of this a circular cylinder is shown as an ellipse (gray color). The maximum scour depth,  $S$ , (which, in this example, is approximately at distance  $D$  onshore of the cylinder) was measured at different times. The results of measurements for different experiments are shown (by different symbols) in dimensionless form in Fig. 17. The maximum scour depth,  $S(t)$ , at a given time is normalized by its maximum equilibrium value  $S^*$  and time

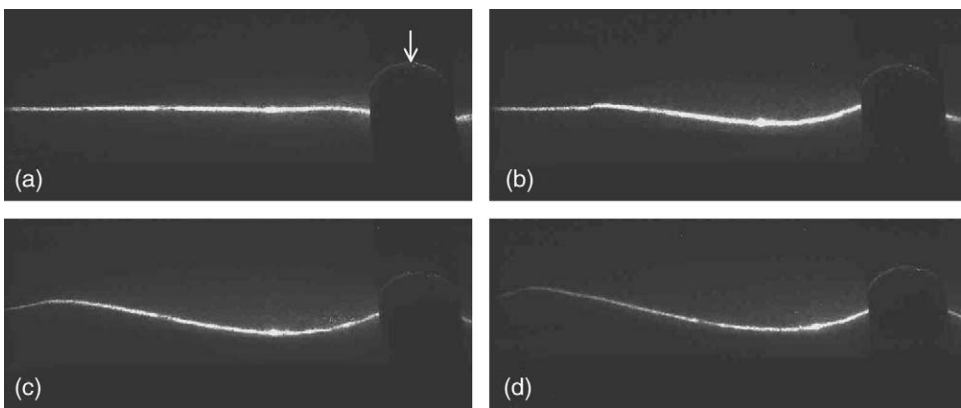


Fig. 15. Four successive photographs from a scour depth measurement experiment where the structured light technique was used. The cylinder itself is poorly visible and its top is shown by arrow in (a). Experimental parameters are:  $D = 5$  cm,  $\omega = 0.4$  Hz,  $\varepsilon_0 = 5$  cm,  $\varepsilon = 6.5$  cm,  $U = 19$  cm s<sup>-1</sup>,  $KC = 8.1$ , and  $Sh = 0.033$ . Time from the beginning of the experiment (in min):  $t = 0$  (a), 15 (b), 100 (c), 140 (d).

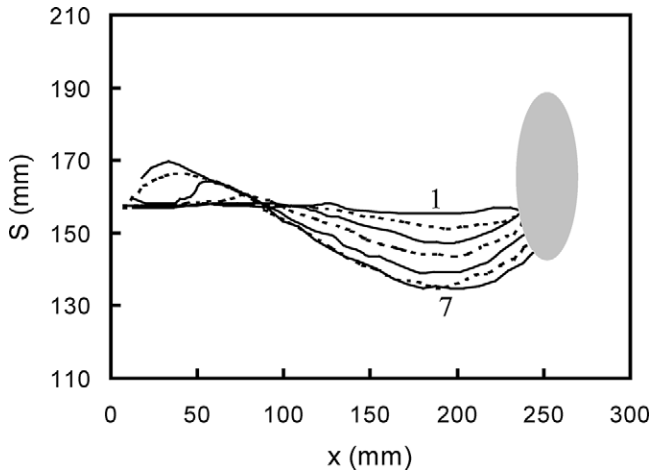


Fig. 16. Scour evolution profiles obtained at the center of the scour gap for the initial scour pattern (regime II). Different scaling is used for the horizontal, X, and vertical, Z, directions, and because of this the circular cylinder is seen as an ellipse (gray color). The origins of X and Z axes are arbitrary. Times for the profiles from 1 to 7 from the beginning of the experiment are (in min):  $t = 0, 1.5, 5, 15, 40, 100, 140$ . Experimental parameters are the same as in Fig. 15. Onshore direction is to the left.

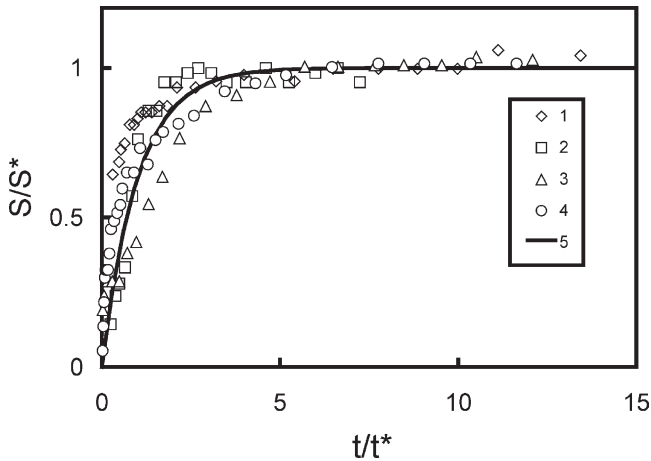


Fig. 17. Dimensionless scour depth at the center of the cylinder,  $S/S^*$ , versus dimensionless time,  $t/t^*$ , for four different experiments. Symbols (1–4) are the results of the measurements, solid line (5) shows the approximation function (17) with  $C = 3300$ . Experimental parameters are:  $D = 5$  cm,  $\omega = 0.4$  Hz,  $KC = 10$ ,  $Sh = 0.076$  (1), 5, 0.2, 14, 0.035 (2), 5, 0.3, 9.4, 0.033 (3), 5, 0.4, 10.5, 0.076 (4).

$t$  is normalized by the characteristic time,  $t^* = C/\omega$ . The value of constant,  $C = 3300$ , was chosen by comparing the measurements with the approximation function

$$S(t)/S^* = 1 - \exp(-t/t^*), \tag{17}$$

which is indicated on Fig. 17 by a solid line. This function was selected based on

arguments similar to that led to Eq. (14). The time,  $T^*$ , at which the system reaches the equilibrium state can be defined as  $T^* = 2t^*$  (time for  $S \approx 0.86S^*$ ). Thus, in our case, the initial scour pattern reaches an equilibrium state after approximately 1000 ( $\approx 6600/2\pi$ ) wave periods, which is the same as time scale for scour around vertical piles to achieve a steady-state (Herbich et al., 1984).

## 5. Conclusions

The results of laboratory experimental program aimed at better understanding the dynamics of scour and burial of heavy three-dimensional cylindrical objects under progressive waves on a sandy bed are presented. The study was motivated by its applicability to the burial/scour of isolated mines on a sandy floor under nonlinear progressive waves such as that occur in shallow coastal waters beyond the region of wave breaking. The aims were: (i) to model this process using laboratory experiments; and (ii) to develop a physical understanding of processes occurring at the sand–object–water interface. Experiments were conducted for a range of flow conditions, which can be characterized by three main dimensionless governing parameters: the Keulegan–Carpenter number,  $KC$ ; Shields parameter,  $Sh$ ; and the dimensionless time. It is shown that, at large times, the scour characteristics reach an equilibrium or a quasi-equilibrium state, wherein, depending on the values of these parameters, different scour regimes around cylinder as well as periodic burial of cylinder under migrating sand ripples appear. The observed behavior was classified into four different basic regimes, namely: (i) no scour, (ii) initial scour, (iii) expanded scour, and (iv) periodic burial. Using this classification, a scour regime diagram was developed and criteria that demarcate these regimes were delineated. Semi-empirical formulae, which permit the calculation of scour depth as a function of time, the equilibrium maximum scour depth and conditions of cylinder burial were also obtained.

## Acknowledgements

This study was supported by the Office of Naval Research, Grants N00014-95-1-0543 and N00014-01-1-0349.

## References

- Batchelor, G.K., 1967. An Introduction to Fluid Dynamics. Cambridge University Press, Cambridge.
- Blondeaux, P., Foti, E., Vittory, G., 2000. Migrating sea ripples. *Eur. J. Mech. B Fluids* 19, 285–301.
- Cevik, E., Yuksel, Y., 1999. Scour under submarine pipelines in waves in shoaling conditions. *J. Waterw. Port Coast. Ocean Eng.* 125 (1), 9–19.
- Faraci, C., Foti, E., Baglio, S., 2000. Measurements of sandy bed scour processes in an oscillating flow by using structured light. *Measurement* 28, 159–174.

- Grilli, S.T., Horillo, J., 1997. Numerical generation and absorption of fully nonlinear periodic waves. *J. Eng. Mech.* 123 (10), 1060–1069.
- Grilli, S.T., Svendsen, I.A., Subramanya, R., 1997. Breaking criterion and characteristics for solitary waves on slopes. *J. Waterw. Port Coast. Ocean Eng.* 123 (3), 102–112.
- Grilli, S.T., Voropayev, S.I., Testik, F.Y., Fernando, H.J.S. Numerical modeling and experiments of wave shoaling over semi-buried cylinders in sandy bottom. In: *Proceedings of 13th International Offshore and Polar Engineering Conference*, Honolulu; accepted for publication.
- Hager, W.H., Del Giudice, G., 2001. Movable bed roughness in alluvial rivers—discussion. *J. Hydraul. Eng.* 127 (7), 627–628.
- Herbich, J.B., Schiller, R.E. Jr., Watanabe, R.K., Dunlap, W.A., 1984. *Seafloor Scour*. Marcel Dekker, New York.
- Kan, M., Kawamura, T., Kuwahara, K., 2001. Numerical study of the sand movement around a cylindrical body standing on the sand. *JSME Int. J. B-Fluids Therm. Eng.* 44 (3), 427–433.
- Nielsen, P., 1992. *Coastal Bottom Boundary Layers and Sediment Transport*. World Scientific, Singapore.
- Roulund, A., Sumer, B.M., Fredsoe, J., Michelsen, J., 1998. 3-D mathematical modeling of scour around a circular pile in current. In: *Proceedings of the seventh International Symposium on River Sedimentation*. Hong Kong, China, 16–18 December, 1998.
- Sarpkaya, T., 1986. Force on a circular cylinder in viscous oscillatory flow at low Keulegan–Carpenter numbers. *J. Fluid Mech.* 165, 61–71.
- Sarpkaya, T., 2002. Experiment on the stability of sinusoidal flow over a circular cylinder. *J. Fluid Mech.* 457, 157–180.
- Sleath, J.F.A., 1984. *Sea Bed Mechanics*. Wiley, New York.
- Snyder, W.H., Castro, P.I., 1999. Acoustic-Doppler-velocimeter evaluation in a stratified tank. *J. Hydraul. Eng.* 125 (6), 595–603.
- Sumer, B.M., Christiansen, N., Fredsoe, J., 1997. The horseshoe vortex and vortex shedding around a vertical wall-mounted cylinder exposed to waves. *J. Fluid Mech.* 332, 41–70.
- Sumer, B.M., Fredsoe, J., Christiansen, N., 1992. Scour around vertical pile in waves. *J. Waterw. Port Coast. Ocean Eng.* 118 (1), 15–31.
- Sumer, B.M., Whitehouse, R.J.S., Torum, A., 2001. Scour around coastal structures: a summary of recent research. *Coast. Eng.* 44, 153–190.
- Van Dyke, M., 1973. *Perturbation Methods in Fluid Mechanics*. The Parabolic Press, Stanford, CA.
- Vittory, G., Blondeaux, P., 1990. Sand ripples under sea waves. Part 2. Finite-amplitude development. *J. Fluid Mech.* 218, 19–39.
- Voropayev, S.I., Cense, A.W., McEachern, G.B., Boyer, D.L., Fernando, H.J.S., 2001. Dynamics of cobbles in the shoaling region of a surf zone. *Ocean Eng.* 28 (7), 763–788.
- Voropayev, S.I., McEachern, G.B., Boyer, D.L., Fernando, H.J.S., 1999. Dynamics of sand ripples and burial/scouring of cobbles in oscillatory flow. *Appl. Ocean Res.* 21 (5), 249–261.
- Voropayev, S.I., Testik, F.Y., Boyer, D.L., Fernando, H.J.S., 2002. Morphodynamics and cobbles behavior in and near the surf zone. *Ocean Eng.* accepted for publication.
- Zdravkovich, M.M., 1997. *Flow Around Circular Cylinders*, vol. 1. Oxford University Press, Oxford.